Springtime photochemical ozone production observed in the upper troposphere over east Asia

Y. Miyazaki,[1] K. Kita,[1] Y. Kondo,[1] M. Koike,[2] M. Ko,[3] W. Hu,[3] S. Kawakami,[4] D. R. Blake,[5] T. Ogawa[4]

Received 4 May 2001; revised 31 August 2001; accepted 31 August 2001; published 14 November 2002.

[1] Aircraft observations of ozone and its precursors (NO, NO_y, CO, and nonmethane hydrocarbons) were made near Japan (26°–44°N) between 21 and 24 April 1998 to investigate the effect of transport and chemistry on the tropospheric ozone over east Asia in spring. The average mixing ratios of ozone and its precursors in the upper troposphere were higher than those observed during February–March 1994. Significantly higher values of CO indicate that the influence of surface sources mediated by convection was large throughout the troposphere during the period. Highly polluted air masses were observed in the upper troposphere at 8–11 km over the Japan Sea on 24 April. These air masses were influenced by cumulus convection associated with a cold front over northeast China about 1 day prior to the observation. However, the majority of observed air masses in the upper troposphere were not directly affected by the recent emissions of the ozone precursors from east Asia. Instead, convection over other regions in the northern midlatitude, followed by long-range transport, affected the abundances of ozone precursors in the upper troposphere. In these air masses, ozone was positively correlated with NO_x and C_3H_8, indicating the effect of photochemical ozone production. The diurnal-average column-integrated rate of ozone production, estimated by a photochemical box model, was larger than the NH average and local stratospheric flux at NH midlatitudes in spring by a factor of 3–20. The net production rates in the majority of the air masses were estimated to be 0.5–4.4 ppbv d^{-1} in the upper troposphere. These results indicate the important role photochemistry plays in controlling the upper tropospheric ozone abundance in spring. *INDEX TERMS:* 0368 Atmospheric Composition and Structure: Troposphere—constituent transport and chemistry; 0345 Atmospheric Composition and Structure: Pollution—urban and regional (0305); 0365 Atmospheric Composition and Structure: Troposphere—composition and chemistry; *KEYWORDS:* Asian outflow, ozone, ozone precursors, convective transport, western Pacific

Citation: Miyazaki, Y., K. Kita, Y. Kondo, M. Koike, M. Ko, W. Hu, S. Kawakami, D. R. Blake, and T. Ogawa, Springtime photochemical ozone production observed in the upper troposphere over east Asia, *J. Geophys. Res.*, *107*, 8398, doi:10.1029/2001JD000811, 2002. [printed *108*(D3), 2003]

1. Introduction

[2] East Asia is the region where rapidly growing industrial activities are causing large increases in emissions of photochemically active pollutants, such as CO, NO_x (= NO + NO_2), and nonmethane hydrocarbons (NMHCs). For example, emissions of NO_x in East Asia are anticipated to increase by a factor of 5 from 1990 to 2020 [*van Aardenne et al.*, 1999]. Emissions of these active pollutants from this continental region have potential impacts on the tropospheric ozone budget over the North Pacific region due to the eastward transport of the polluted air masses in the free troposphere by strong westerlies at midlatitudes. Knowing the impact of surface pollutants in the present-day atmosphere will enable us to anticipate how ozone will respond to future changes.

[3] The transport of pollutants from east Asia to the North Pacific is generally most effective in spring, due to a combination of active convection over the continent and strong westerlies [*Merrill*, 1989]. Aircraft observations showed high levels of total reactive nitrogen (NO_y) in the free troposphere over the Hawaiian region in spring, probably due to export from northern latitude continental surface regions [*Ridley et al.*, 1997]. Transport of Asian pollution, such as CO and NMHCs, to the northwestern contiguous United States during spring was observed by ground-based

[1]Research Center for Advanced Science and Technology, University of Tokyo, Tokyo, Japan.
[2]Earth and Planetary Science, Graduate School of Science, University of Tokyo, Tokyo, Japan.
[3]Atmospheric and Environmental Research, Inc., Lexington, Massachusetts, USA.
[4]Earth Observation Research Center, National Space Development Agency of Japan, Tokyo, Japan.
[5]Department of Chemistry, University of California, Irvine, California, USA.

0148-0227/02/2001JD000811

measurements [*Jaffe et al.*, 1999]. In addition to the transport of pollution, solar ultraviolet radiation intensifies as spring advances because of changes in solar zenith angle and total ozone [*Yienger et al.*, 1999]. Active photochemistry combined with transport can contribute to the springtime increase of ozone in the free troposphere over east Asia, as shown by the recent analysis of ozonesonde data obtained over Japan [*Logan*, 1999].

[4] In situ and remote measurements of an extensive suite of trace gases were made over the western Pacific during the Pacific Exploratory Mission-West (PEM-W)-A in September–October 1991 and PEM-W-B in February–March 1994 to investigate chemical processes and long–range transport of trace species over the northwestern Pacific and to estimate the impact of human activities on these species over this region [*Hoell et al.*, 1996, 1997]. Comparisons of these data indicate that the air masses sampled in early spring (PEM-W-B) were more polluted than those sampled in fall (PEM-W-A). A first indicator for the effects of surface pollutants is the hydrocarbon data. Below 5 km, the mixing ratios of hydrocarbons, which originated from the continental surface, were much larger during PEM-W-B than those during PEM-W-A due to the strong outflow from the Asian continent [*Blake et al.*, 1997; *Gregory et al.*, 1997; *Kondo et al.*, 1997a; *Talbot et al.*, 1997]. However, in the upper troposphere, mixing ratios of pollutants were smaller than those below 5 km during PEM-W-B because of the lack of deep convection, which transports pollutants from the lower troposphere, as is typical for winter/early spring [e.g., *Newell et al.*, 1997]. An implicit assumption in this discussion is that air parcels below/above 5 km sampled by the aircraft came from below/above 5 km upwind. Thus the trace gas abundance measured by the aircraft over the Pacific could be used as a proxy for that over the Asian continent.

[5] A second indicator of the effects of Asian outflow is the column ozone budget. Photochemical model calculations indicate that net ozone production occurred between 0–12 km at 20°–50°N during PEM-W-B, in contrast to PEM-W-A where net ozone loss at lower altitudes balanced net production at higher altitudes at 18°–42°N [*Crawford et al.*, 1997].

[6] Comprehensive observations in April, when stronger convective activities are expected to transport air from below 5 km to the upper troposphere, would better quantify the role of sources on springtime ozone increases in the upper troposphere over east Asia. As a part of the Biomass Burning and Lightning Experiment (BIBLE) campaigns, three aircraft observation flights were made near Japan in April 1998, called BIBLE T. Major objectives of this study were (1) to study the influence of continental outflow on the distributions of trace gases up to the tropopause over east Asia in April, and (2) to study the relative contribution of photochemical production to the spring increase of tropospheric ozone over these regions. In this paper, effects of convective transport and photochemical ozone production in the upper troposphere are discussed based on the observed data.

2. Aircraft Observations

[7] During the BIBLE T experiment, atmospheric sampling was conducted aboard the Gulfstream (G-II) aircraft at

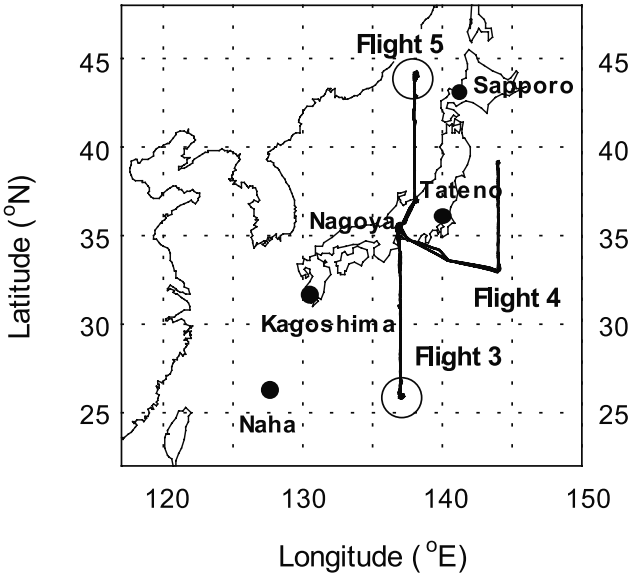

Figure 1. The flight tracks of flight 3 (21 April), flight 4 (22 April), and flight 5 (24 April). Open circles show the sites where vertical profiles were obtained on flight 3 and flight 5. The locations of the observation sites of the ozonesondes: Sapporo (43.1°N, 141.3°E), Tateno (36.1°N, 140.1°E), Kagoshima (31.6°N, 130.6°E), and Naha (26.2°N, 127.7°E) are also presented.

26°–44°N near Japan. The base of operations was Nagoya International Airport. The horizontal flight tracks are shown in Figure 1. The intensive aircraft observations were carried out on three flights on 21, 22, and 24 April after two test flights. The G-II aircraft flew from Nagoya south to 26°N over the Pacific on April 21 (flight 3). On 22 April (flight 4), the aircraft flew east and then went north, over the western Pacific. Measurements were made up to 44°N over the Japan Sea on 24 April (flight 5). The G-II aircraft flew mostly in the upper troposphere above 7 km and the maximum flight level was 13.2 km. Altitude profiles of constituents were also obtained at two locations as shown in Figure 1.

[8] During BIBLE T, ozone, CO, NO, NO_y, H_2O, NMHCs, and meteorological parameters were measured. The instruments aboard the aircraft and their characteristics are listed in Table 1. Ozone was measured by a UV absorption photometer with a detection limit of 3 ppbv at 13 km and less than 3 ppbv at lower altitudes [*Kita et al.*, 2002]. The CO mixing ratio was measured by an automated gas chromatograph (GC) with a reduction gas detector (RGD) [*Kita et al.*, 2002]. It was measured with a time interval of 20 s using three independent GC-RGD units. Because of the uncertainty of the CO standard gases used for the GC-RGD during this experiment, the accuracy of the 20-s data was 10% at 200–300 ppbv, 20% at 100–200 ppbv, and 30% at 0–100 ppbv. NO and NO_y measurements were made using a chemiluminescence technique with a 1-s time resolution. The precision of the 10-s NO and NO_y measurements at 10 km was 3 and 5 pptv for NO and NO_y values of 100 and 200 pptv, respectively [*Kondo et al.*, 1997b; *Koike et al.*, 2000]. The actinic flux was measured using UV radiometers to calculate the photolysis rate

Table 1. Parameters and Measurement Techniques for the BIBLE T

Species/Items	Techniques	Sampling Time Interval	Precision (10 s)	Accuracy
O_3	UV absorption	1 s	<3 ppbv	5%
CO	GC/HgO-reduction	20 s	2 ppbv	5%
NO, NO_y	Chemiluminescence	1 s	3 pptv (NO), 5 pptv (NO_y)	8% (NO), 17% (NO_y)
Actinic Flux	UV radiometer	1 s	2×10^{-4} s^{-1}	8%
H_2O	Dew point hygrometer	10 s	0.2–1.0°C	<5%
NMHCs	Whole air sampling/GC	5 min	<3 pptv	2–20%

coefficient of NO_2 ($J(NO_2)$) [*Junkerman et al.*, 1989]. The $J(NO_2)$ filter radiometer was absolutely calibrated by Meteorologie Consult (Glashütten, Germany) and the precision was 2×10^{-4} s^{-1} for 10-s data. The photostationary state of NO_2/NO ratios above 8 km were calculated using the measured values of ozone, temperature, pressure, and $J(NO_2)$. The ratios were calculated for solar zenith angles lower than 67°. The NO_x mixing ratios were calculated from these NO_2/NO ratios and the observed NO mixing ratios. The dew point was measured with two different types of dew point hygrometers (model 1011A provided by General Eastern and model CR-2 provided by Buck Research). The lower detection limits are −75°C for the 1011A and −95°C for the CR-2. The H_2O mixing ratios were derived from these measurements over the ranges of 1–100,000 ppmv (1011A) and 0.01–27,000 ppmv (CR-2). Whole air samples were collected into 2-L stainless steel sampling canisters and more than sixty samples were obtained per flight. The samples were analyzed for a suite of NMHCs in the laboratory at the University of California, Irvine [*Blake et al.*, 1996].

3. Results and Discussion

3.1. Altitude Profiles

[9] Figures 2a–2e show the altitude distributions of ozone, CO, C_3H_8, NO, and NO_y observed during 21–24 April (flights 3–5). Ozone, CO, NO, and NO_y values averaged for 10-s were used. The median values are also shown in the right panel with 1-km resolution. Data obtained during takeoff and landing in Nagoya below 2 km were excluded because these data showed a large variability due to local pollution. Data below 2 km obtained over the ocean during fights 3 and 5 were used. The bars shown in the median profiles indicate the range spanned by 67% of the data around the median values. Because the number of data below 2 km is limited, the median values below 2 km may not be representative for the BIBLE T period. During these flights, the measurements were made below the tropopause, which was defined by the temperature obtained by the routine radiosonde observations at several sites in Japan by the Japan Meteorological Agency (JMA). Figures 2a–2e also show altitude profiles of the median values observed during PEM-W-A and PEM-W-B for comparison. The PEM-W-A data obtained at the same latitudes (26°–44°N) as for BIBLE T were used. The data used in this comparison were obtained during flights 5–13 (17 September to 6 October 1991). The PEM-W-B data shown in Figures 2a–2e were limited to 20°–30°N because the tropopause height north of 30°N was as low as 8–9 km [*Koike et al.*, 1997], and the data obtained above 8 km north of 30°N were from the lowermost stratosphere. In order to compare BIBLE T data with those at 0–12 km in the troposphere, the PEM-W-B data obtained north of 30°N

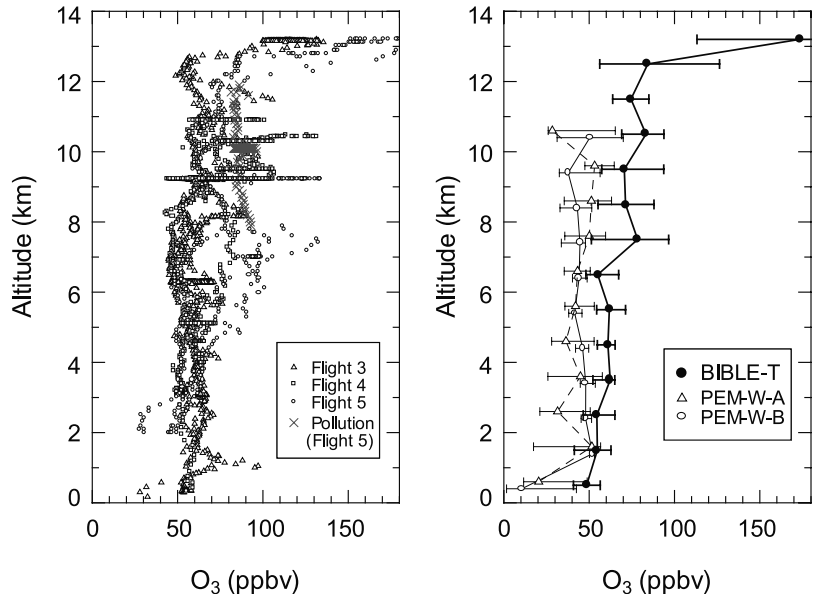

Figure 2a. Altitude profiles of the observed ozone mixing ratios during BIBLE T. The 10-s averaged data was used. The median values shown in the right panel are compared with those observed during PEM-West A (September–October 1991) and PEM-West B (February–March 1994). The bars indicate the central 67% values. Highly polluted air masses observed during flight 5 are also shown by crosses.

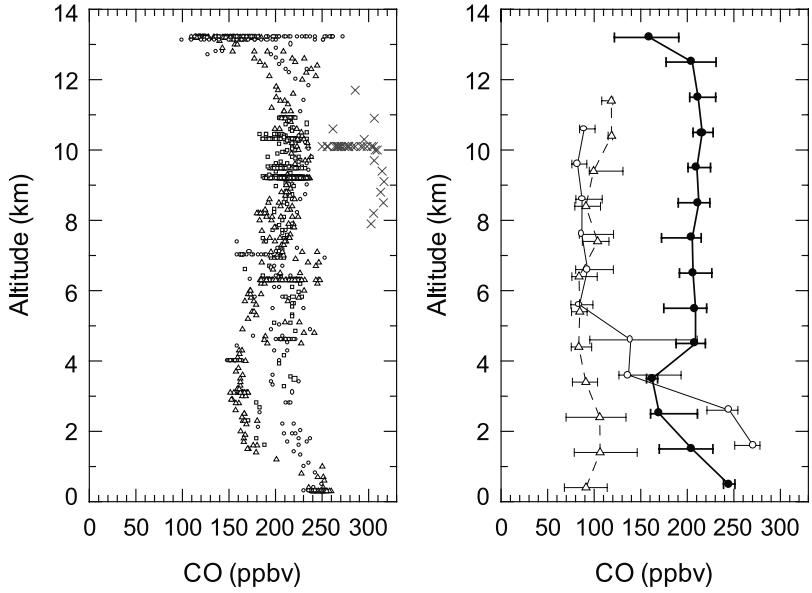

Figure 2b. Same as Figure 2a but for CO.

were excluded. The PEM-W-B data used were obtained during flights 7, 8, and 12–16 (13 February to 7 March 1994). Both of the PEM-W-A and B flights used here were made at the same longitude (120°–150°E) as BIBLE T. During both PEM–W-A and PEM-W-B, NO and NO_y measurements were made by Nagoya University (NU) using a chemiluminescence technique [*Kondo et al.*, 1996, 1997b] and by the Georgia Institute of Technology using a laser-induced fluorescence technique [*Sandholm et al.*, 1997]. Comparisons of NO_y measured by NU and the sum of reactive nitrogen species showed good agreement over the Pacific [*Kondo et al.*, 1997a] and the North Atlantic (slope >0.9 and $r^2 \approx 0.9$) [*Talbot et al.*, 1999]. In this paper, the NO and NO_y values measured by NU during PEM-W-A and PEM-W-B were used. The median ozone mixing ratios during BIBLE T were 71–84 ppbv at 7–13 km and 55–62 ppbv below 7 km. The ozone concentrations during BIBLE T were higher than those observed during PEM-W-A and PEM-W-B, by 11–35 ppbv at all altitudes. Although all the data were obtained below the tropopause, stratospheric intrusion likely influenced the median ozone value of 170 ppbv around 13 km.

[10] Figure 3a compares the median ozone mixing ratios during BIBLE T with ozonesonde data obtained in Japan in April for the years 1993–1997. The ozonesonde observations were routinely conducted at four stations in Japan: Sapporo (43.1°N, 141.3°E), Tateno (36.1°N, 140.1°E), Kagoshima (31.6°N, 130.6°E), and Naha (26.2°N, 127.7°E), about once a week by JMA. Data obtained above the tropopause were excluded. The BIBLE T data may not be representative of conditions in spring because the data were obtained over a period of three consecutive days, so

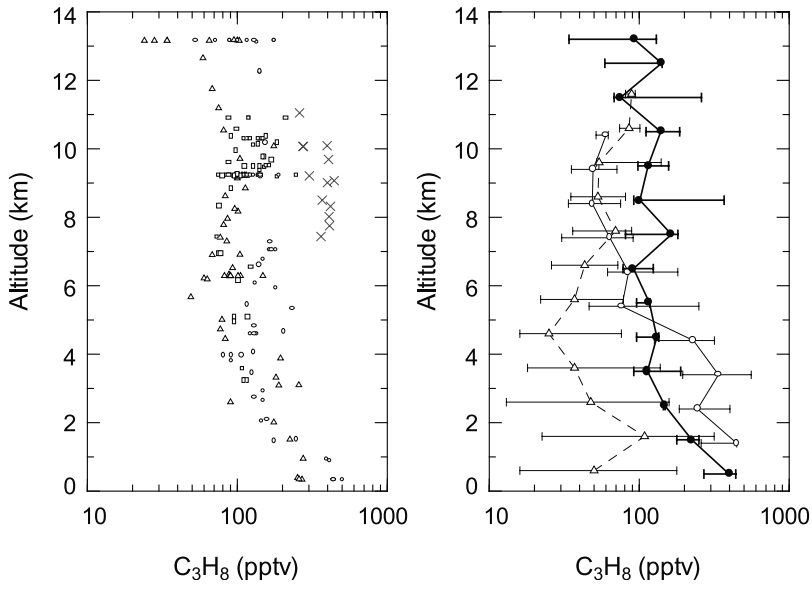

Figure 2c. Same as Figure 2a but for C_3H_8. The 5-min data were used.

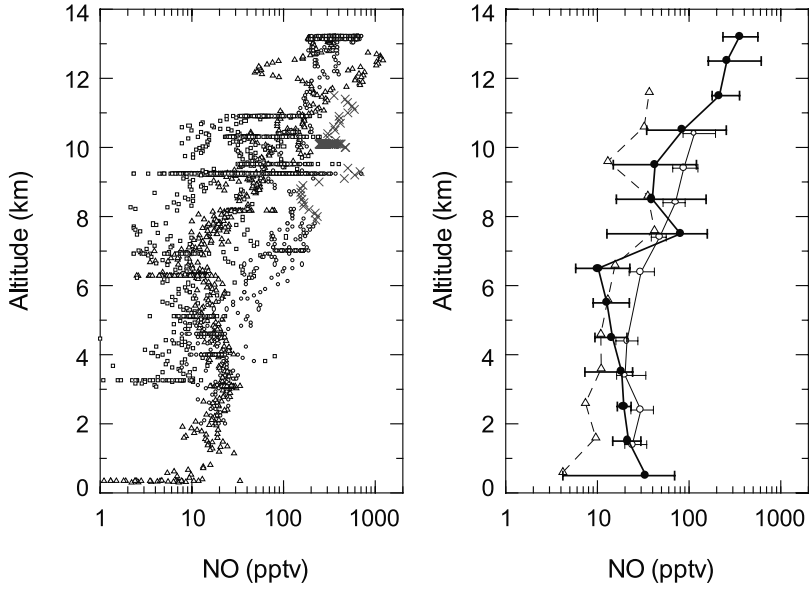

Figure 2d. Same as Figure 2a but for NO. Several spikes due to aircraft emissions larger than 800 pptv were excluded.

the results might well have been influenced by synoptic scale events. However, comparison with ozonesonde data shows that the aircraft ozone median values agree well with the median values of the 5-year ozonesonde data between 2–12 km (50–85 ppbv), within a variability of ±15 ppbv. The median ozone mixing ratios during PEM-W-A and PEM-W-B also agree with those of the 5-year ozonesonde data (30–65 ppbv) within a variability of approximately ±20 ppbv for September–October (Figure 3b) and for February–March (Figure 3c), respectively. Therefore the difference in the ozone levels during BIBLE T and PEM-W-B should be mainly due to the lack of convective activities during PEM-W-B compared to BIBLE T, which is a reflection of the seasonal variation of synoptic scale meteorology.

[11] During BIBLE T, the CO mixing ratios at 5–12 km were fairly constant at about 200 ppbv, which were higher than those observed during PEM-W-A and PEM-W-B by a factor of 1.5–2, as shown in Figure 2b. At 2–5 km, the CO mixing ratios during BIBLE T were similar to those during PEM-W-B, but higher than those during PEM-W-A by a factor of 1.5, as anticipated from the seasonal variation at the surface: a maximum in late winter/spring and a minimum in summer/early autumn at remote sites in the Northern Hemisphere [*Novelli et al.*, 1994, 1998]. In addition to the seasonal cycle of CO at the surface driven by the reaction with OH, increased CO emissions from biomass burning in late winter-spring in the Northern Hemisphere [e.g., *Galanter et al.*, 2000] could enhance the whole CO column as observed during BIBLE T. It

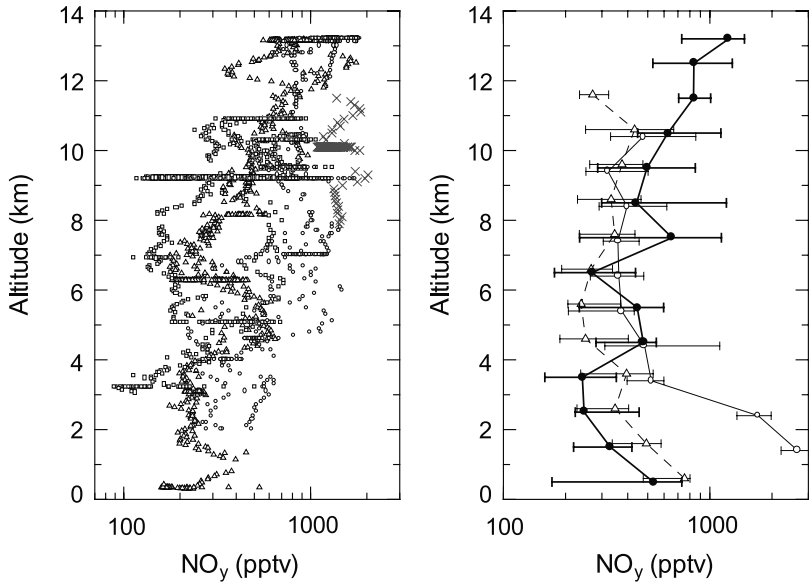

Figure 2e. Same as Figure 2a, but for NO_y. Several spikes larger than 2.5 ppbv were excluded.

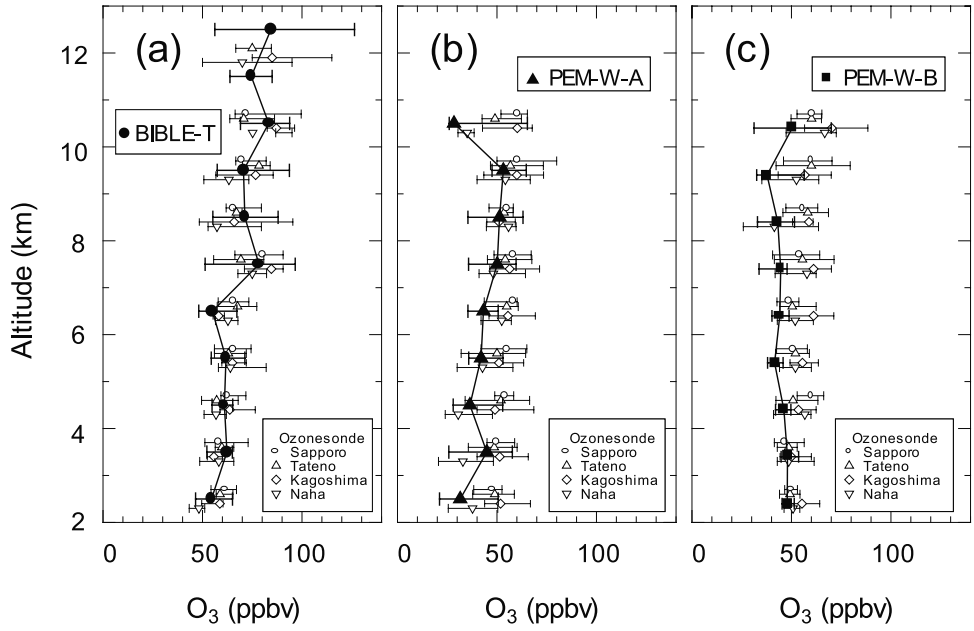

Figure 3. (a) Observed ozone mixing ratios during BIBLE T compared with the median ozonesonde values at four Japanese stations in April. (b) PEM-W-A data compared with the ozonesonde data in September–October. (c) PEM-W-B data compared with the ozonesonde data in February–March for 1993–1997. The bars indicate the central 67% values.

should be noted that the vertical gradient of the CO mixing ratios at 4–8 km during BIBLE T and PEM-W-A was much smaller than that during PEM-W-B. The small vertical gradient was also seen for C_3H_8 (Figure 2c) during BIBLE T. The lifetimes of CO and C_3H_8 are roughly 2 months and 10±6 days, respectively (depending on the OH concentration). Since both CO and C_3H_8 are mainly emitted from the surface, these altitude distributions indicate that major convective activity occurred at least once within 10 days prior to the flights and throughout the troposphere at northern midlatitudes. Profiles for shorter-lived hydrocarbons indicate that 15% of the samples experienced convective activity within the last 2 days, as discussed in section 3.2.

[12] The median NO and NO_y mixing ratios at 2–7 km were 10–20 pptv and 240–480 pptv, respectively (Figures 2d and 2e). They were similar to those observed during PEM-W-A and PEM-W-B. The median NO and NO_y mixing ratios at 7–13 km were 40–350 pptv and 440–1230 pptv, respectively. The NO values above 9 km during BIBLE T were much higher than those during PEM-W-A, although they were more or less similar to those during PEM-W-B. The increase in the NO mixing ratios with altitude has also been previously observed [*Liu et al.*, 1980; *Kley et al.*, 1981; *Drummond et al.*, 1988; *Ridley et al.*, 1994]. This increase is due to the longer chemical lifetime of NO_x and additional sources of NO_x in the upper troposphere, such as lightning, aircraft emissions, and stratospheric intrusions. The BIBLE T NO_y mixing ratios were similar but slightly higher than those during PEM-W-A and PEM-W-B above 7 km. There is no simple explanation for the lower concentrations of NO at 2–7 km during BIBLE T in contrast to the higher concentrations of CO and C_3H_8, because of the shorter lifetime of NO compared to those of CO and C_3H_8, together with the fewer number of data samplings below 7 km than above.

3.2. Identification of Air Masses Influenced by Pollutants From East Asia

[13] The origins of air masses sampled in the upper troposphere were investigated using 10-day isentropic back trajectories. The trajectories were calculated with the trajectory model developed by *Matuzono et al.* [1998], using the European Centre for Medium-range Weather Forecasts (ECMWF) 2.5° resolution data. Figure 4 gives a summary of trajectories for air masses sampled above 7 km. Almost all the air masses were transported over the Asian continent by the dominant westerlies in the upper troposphere at northern midlatitudes. Above 10 km, the air masses were transported from over the Atlantic Ocean and even the U.S. continent within 10 days. Although the range of latitude that the trajectories passed varied from flight to flight, the flow of the air masses were mostly confined to the 15°–45°N latitude band. These trajectories suggest that the observed air masses were not significantly affected by high-latitude or tropical air. The air masses identified to be strongly influenced by east Asian pollution are discussed below in this section.

[14] The profiles of C_3H_8 indicate that convective activities in April occurred with sufficient frequency that they maintained high upper tropospheric concentrations of gases with atmospheric lifetimes of 10 days. The C_2H_2/CO ratio can be used as an indicator of the relative degree that air masses have been photochemically processed on a timescale of 1–3 weeks, which is the photochemical lifetime of C_2H_2 [e.g., *Smyth et al.*, 1996]. In the study of remote western Pacific air during PEM-W-A, C_2H_2/CO values of 1 pptv/ppbv or lower were identified as photochemically well-aged

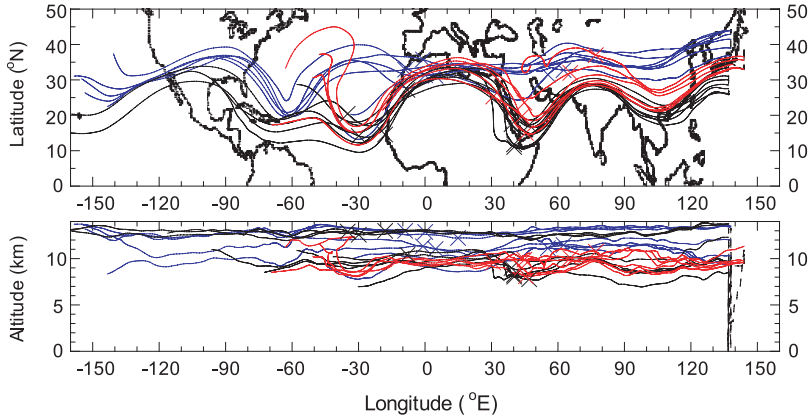

Figure 4. Summary of 10-day isentropic back trajectory calculations along flight tracks for flight 3 (black), flight 4 (red), and flight 5 (blue) at altitude above 7 km. Crosses show 5-day intervals on each trajectory.

air [*Smyth et al.*, 1996]. Although the ratio contains uncertainty due to the complexity of sources and atmospheric mixing, the median C_2H_2/CO value of 1.2 pptv/ppbv above 7 km indicates that a majority of the air masses were photochemically aged. Convective transport over the Asian, European, and North American continents all contribute to the observed high upper tropospheric concentrations. The effects of emissions and vertical transport could not be separated from each continent due to the complexity of source distributions and transport, given lifetimes of 10 days during which the air masses were transported over very long distances in the free troposphere. However, the origin of some air masses observed in the upper troposphere on 24 April has been identified to be the boundary layer over east Asia as detailed below.

[15] For flight 5, highly polluted air masses were observed between 8–11 km at 43°–44°N, 137°E, over the Japan Sea. The mixing ratios of CO, ozone, C_3H_8, NO, and NO_y observed in these air masses are summarized in Table 2. The values of these species were elevated above the median values observed during BIBLE T. In addition, large enhancements of short-lived n-C_4H_{10} up to 113 pptv associated with the relatively high values of the C_2H_2/CO ratios (2.0–2.8) were also observed. The median n-C_4H_{10} value in these air masses was 62 pptv, which was significantly higher than the value of 12 pptv in the other air masses. The median NO_x/NO_y ratio of 0.29 was also 3 times larger than that in the other air masses. The photochemical age of these air masses should be on the order of 1–3 days, which is the photochemical lifetime of n-C_4H_{10}. In spite of the moderately high ozone mixing ratios (90 ± 6 ppbv), ozone was not significantly correlated with CO, NO, NO_y, and NMHCs (C_2H_6 and C_3H_8) in these air masses (not shown). Photochemical production of ozone cannot proceed sufficiently on a timescale of 1–3 days in these "freshly" polluted air masses.

[16] In order to identify the location of the convection, 5-day backward trajectories, combined with the cloud image data obtained by the Japanese Geostationary Meteorological Satellite-5 (GMS-5), were used. The resolution of the cloud images was 0.25° in latitude and longitude for the infrared (IR)-1 (λ = 10.5–11.5 μm) and IR-2 (λ = 11.5–12.5 μm) channels. The difference in the brightness temperature (DBT) between the 2 channels depends sensitively on the optical thickness of the clouds. In this analysis, optically thick clouds were defined as those with DBT values smaller than 1 K [*Inoue*, 1985, 1989]. The air temperature at a position of an air mass along its back trajectory was compared with the brightness temperature at the position for each 1-hour period. The air mass was considered to have been affected by the outflow of convective clouds if the brightness temperatures were lower than the air temperatures at the time when the horizontal locations of the air masses overlapped with those of the optically thick clouds.

[17] Figure 5 shows the air temperature of these air masses along the back trajectories and the average brightness temperature at the same horizontal grid. It can be seen that the air mass encountered optically thick clouds at longitudes of 117°–120°E, 36–48 hours prior to the aircraft measurement. Figure 6 shows temporal variation of cloud distributions for the latest 2 days prior to the observations with a time interval of about 12 hours. The air masses were thus identified as having been convected over northeastern China. The cloud image and trajectories indicate that the air masses moved eastward along with cumulus clouds associated with a developing low-pressure system. The age of the convective plume of 1–1.5 days, estimated from the meteorological analysis, is consistent with the photochemical age estimated from the concentrations of short-lived n-C_4H_{10}. Ozone production would continue during the eastward transport of these air masses. This case study demonstrates that

Table 2. Observed Values of Chemical Species Between 8 and 11 km at 43°–44°N, 137°E Over the Japan Sea on 24 April[a]

Chemical Species	CO, ppbv	O_3, ppbv	C_3H_8, pptv	NO, pptv	NO_y, pptv
Japan Sea (24 April)	250–317	83–96	260–442	160–680	1080–2030
Median values during BIBLE T	210	78	121	130	541

[a] Median values at 8–11 km during BIBLE T are also shown for reference.

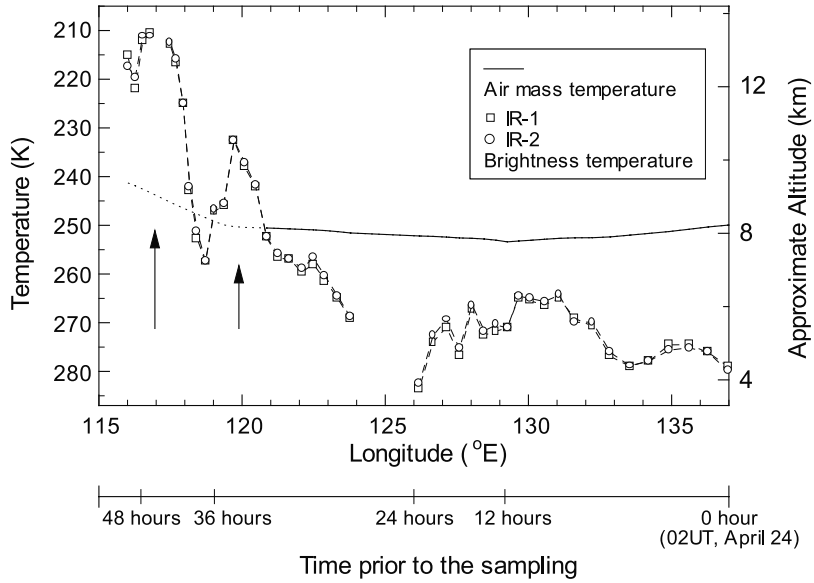

Figure 5. Temporal and longitudinal variation of the air mass temperature and brightness temperature along 48-hour back trajectories. The brightness temperature had been lower than the air temperature during 36 hours before the observation and was higher than the air temperature before that. Cumulus clouds are identified using the IR-1 and IR-2 channels (see text). The results showed that the back trajectories encountered cumulus clouds about 36 hours before the observation (shown by arrows), suggesting that the air masses were affected by cumulus convection within the previous 1–2 days. The trajectories in the convective clouds are shown by a dotted line.

convective transport associated with a cold front over east Asia can transport a significant amount of the ozone precursor species from the boundary layer to the upper troposphere in spring. A global 3-D model study of *Bey et al.* [2001] has suggested the importance of frontal lifting as a mechanism of the export of CO from China and formation of an Asian pollution plume in the middle troposphere over the Pacific during PEM-W-B.

3.3. Correlations Analysis

[18] We now examine the correlations of different species above 7 km. In this analysis, we excluded data strongly impacted by the recent convection over the northeastern part of China as discussed in 3.2. The meteorological analysis using the same method indicates that the rest of the air masses were not impacted by recent (within 2 days) convection over east Asia, consistent with the low C_2H_2/CO ratios in the majority of the sampled air masses, as discussed in 3.2.

[19] Also as described in 3.1, some influence of stratospheric intrusions was seen around 13 km, just below the tropopause. The CO mixing ratios at these altitudes were 110–160 ppbv, which was lower than those below 13 km. The low H_2O mixing ratios of 15–60 ppmv (not shown) were similar to those observed in stratospheric air masses at midlatitudes [*Kondo et al.*, 1997a; *Kotamarthi et al.*, 1997]. The ozone and NO_y mixing ratios were mostly higher than 100 ppbv and 500 pptv, respectively, as seen in Figures 2a and 2e. These low values of CO and H_2O, together with high values of ozone and NO_y, indicate that the air masses obtained around 13 km were affected by stratospheric input. These stratospherically influenced data were also excluded from the following analysis.

[20] Correlations among ozone and its precursors can be used to investigate contributions of emissions of precursors from continents. The NO_x mixing ratios derived from the measured NO and the NO_y mixing ratios in these air masses are plotted against the C_3H_8 mixing ratios in Figure 7. The NO_y mixing ratios are well correlated with the C_3H_8 mixing ratios ($r^2 = 0.67$). On the contrary, NO_y showed no significant correlations with CO (not shown). The lifetime of NO_y, after emission from the surface, is controlled by removal of HNO_3 by heterogeneous processes. These results show that effective loss of NO_y occurred with a time constant similar to the lifetime of C_3H_8 (about 10 days), which is determined by the reaction with OH. Because the lifetime of CO is about 2 months, NO_y is lost much more rapidly than CO, reducing the NO_y-CO correlation in moderately aged air masses. Mixing of fresh pollution or moderately aged air with background air (well-aged air) will further weaken the NO_y-CO correlation because NO_y is more depleted than CO in background air.

[21] The NO_x-C_3H_8 correlation is somewhat more scattered ($r^2 = 0.48$) than the NO_y-C_3H_8 correlation. Conversion of NO_x into HNO_3 and PAN mainly controls the lifetime of NO_x after emission from the surface and transport to the upper troposphere. The lifetime of NO_x is shorter than NO_y and C_3H_8, leading to the NO_x-C_3H_8 correlation more scattered than the NO_y-C_3H_8 correlation.

[22] These results suggest that NO_x and NO_y in these air masses were supplied dominantly by the upward transport of polluted air near the surface within the photochemical lifetimes of C_3H_8. However, during upward transport by deep convection, lightning can add a significant amount of NO to the polluted air masses rich in NO_x, CO, and NMHCs [e.g., *Liu et al.*, 1999]. Therefore these correlations cannot,

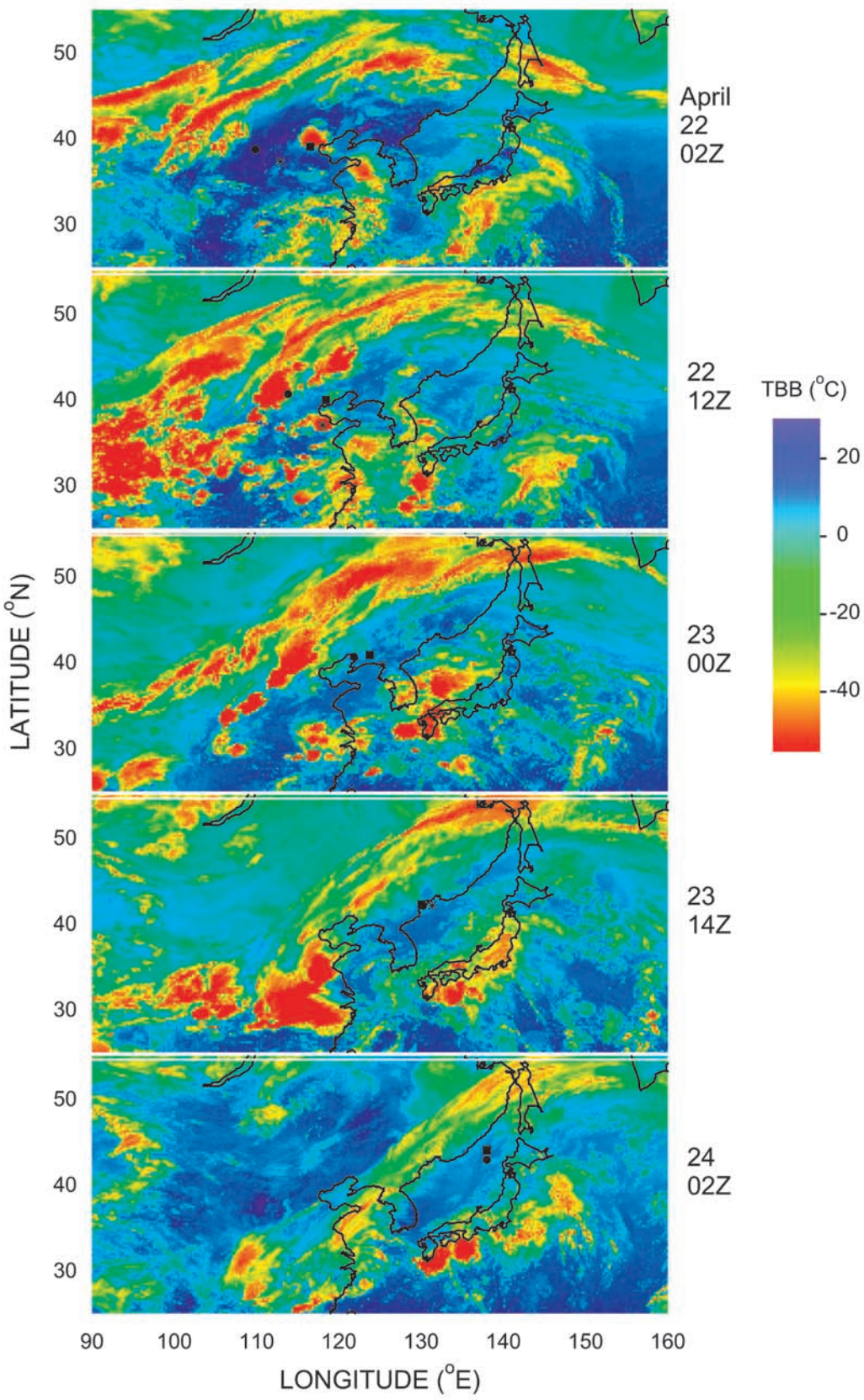

Figure 6. Temporal variation of cloud distributions during a time interval of about 12 hours before the observation. Marks indicate the positions of air masses in which enhancements of ozone precursors were observed at 8–11 km. They were estimated by the trajectory calculations.

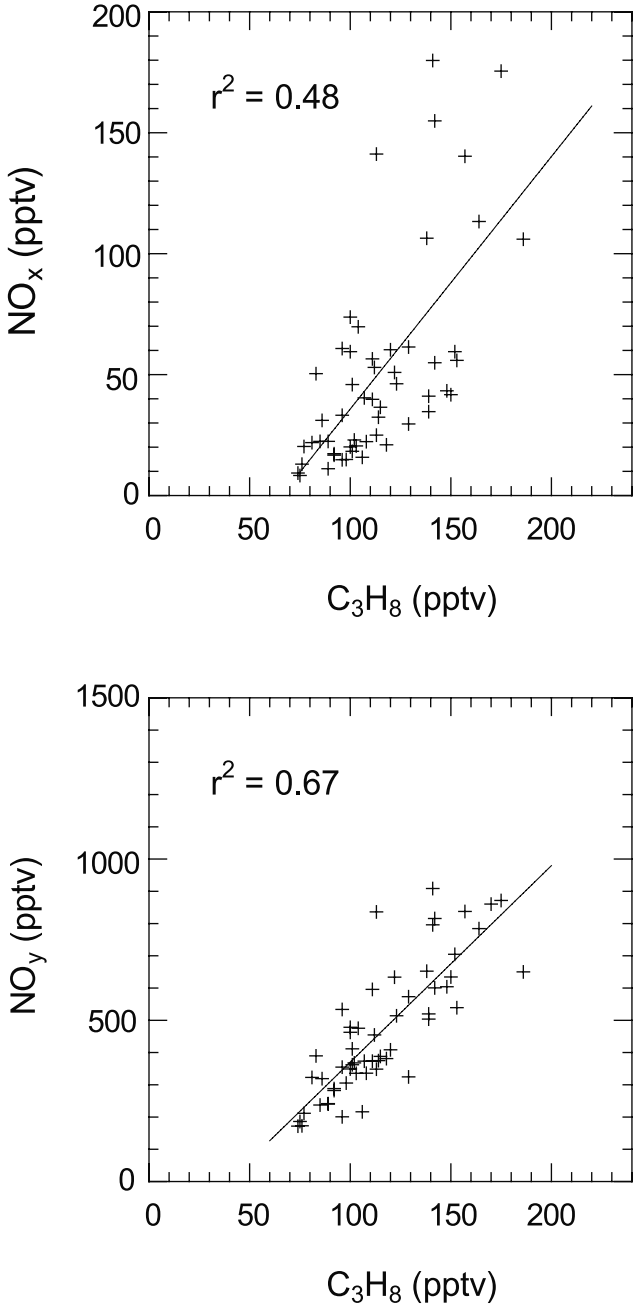

Figure 7. Scatterplots of C_3H_8 versus (top) NO_x and versus (bottom) NO_y. All the data above 7 km were used after excluding the data from highly polluted air masses and stratospheric air masses (see text).

by themselves, unambiguously separate the contribution of lightning from the production by anthropogenic activities near the surface.

[23] Ozone was correlated with NO_y ($r^2 = 0.66$) and C_3H_8 ($r^2 = 0.56$) in these air masses independent of the flights, as shown in Figures 8 and 9. Generally, a tight, positive correlation between ozone and NO_y indicates air masses that have been photochemically processed in the troposphere [*Buhr et al.*, 1996; *Daum et al.*, 1996] and/or influenced by downward transport from the stratosphere [*Murphy et al.*, 1993; *Weinheimer et al.*, 1993]. The slope of

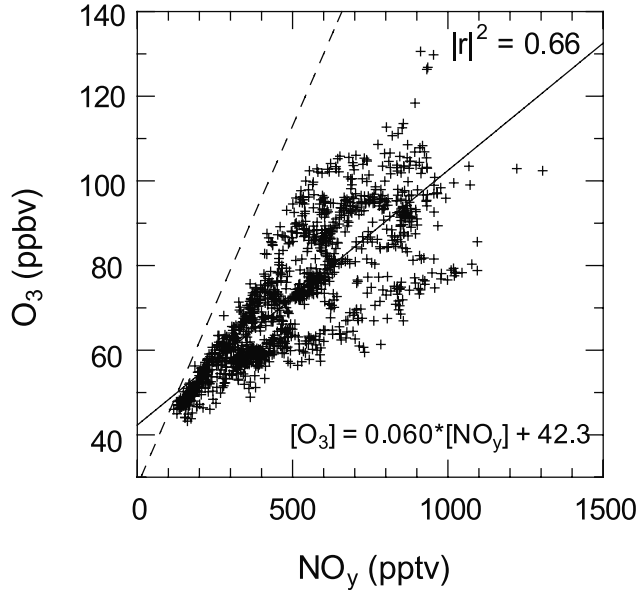

Figure 8. Scatterplot of ozone versus NO_y. Data used are the same as those in Figure 5. The dashed line represents a typical slope of regressions from the middle to northern latitude lower stratosphere [*Murphy et al.*, 1993; *Buhr et al.*, 1996].

the regression line (0.060 ppbv ozone per pptv NO_y) is smaller by a factor of 3 than the typical values obtained in the lower stratosphere at northern midlatitudes [*Murphy et al.*, 1993; *Koike et al.*, 1997] (Figure 8). In addition to this, the positive correlations of NO_x and NO_y with C_3H_8, as well as the high mixing ratios of CO and C_3H_8, excludes significant effects of stratospheric air. Mixing of air high in NO_y, C_3H_8, and O_3 with clean air can produce the correlations discussed above. However, high values of

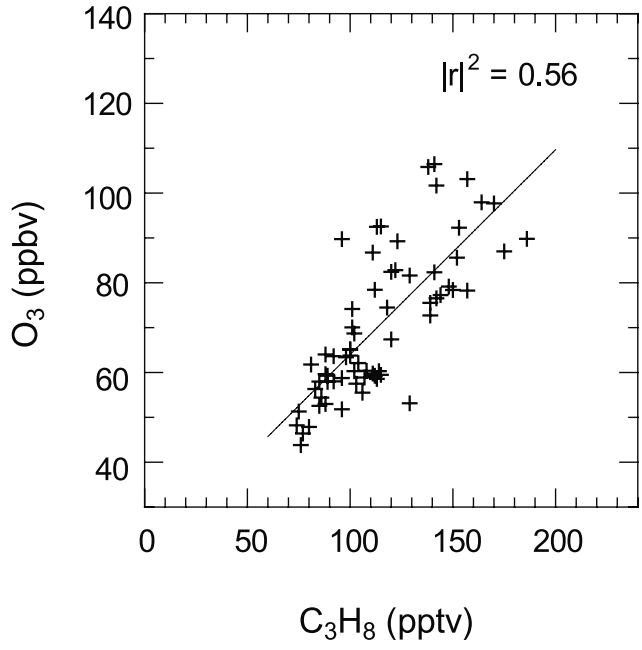

Figure 9. Scatterplot of ozone versus C_3H_8. Data used are the same as those in Figure 5.

Table 3. Budget of Tropospheric Ozone During BIBLE T[a]

	Altitude, km			
	0–2	2–7	7–13	0–13
Number of model points	32	114	301	447
Column rates, 10^{10} mol cm^{-2} s^{-1}				
Production (P) O_3	29 (−12/+21)	22 (−2/+16)	23 (−5/+14)	74 (−32/+51)
Loss (L) O_3	25 (−9/+5)	30 (−10/+20)	6 (−1/+2)	61 (−21/+27)
Net (P-L)	8 (−20/+16)	−9 (−8/+12)	16 (−9/+13)	17 (−38/+41)

[a] Median diurnal average rates and central ±67% values calculated by the model. Because entries are medians, Net (P-L) and $P(O_3)$-$L(O_3)$ are not identical.

ozone, with simultaneously high NO_x and C_3H_8, are still required to produce the observed correlations, indicating that photochemical production of ozone had occurred in sampled air masses.

[24] Ranges of the ozone and NO_y values during BIBLE T were similar to those in the observed air masses in the free troposphere over Hawaii in April and May [*Ridley et al.*, 1997]. While trajectories arriving over Hawaii frequently passed over the Asian continent, our results indicate that these air masses were not necessarily or solely affected by the surface sources of the Asian continent, but may also have been affected by other continents in the northern midlatitudes.

3.4. In Situ Production of Ozone in the Troposphere

[25] Although the correlations between ozone and its precursors demonstrate the effects of photochemical ozone production, the altitude region where the ozone production mainly occurred cannot be identified. As already discussed, the concentrations of trace species with lifetimes longer than 10 days were strongly influenced by convection in April. Ozone in the upper troposphere may not necessarily have been produced at the altitudes of sampling, but may have been transported from lower altitudes where ozone can be produced, depending on the levels of the ozone precursors and the length of time during which the air masses stayed there. The contribution of the in situ ozone production at the time of the observation was assessed by calculating the diurnal average of the net ozone production rates. The Atmospheric and Environmental Research, Inc. (AER) photochemical box model [*Kotamarthi et al.*, 1997; *Ko et al.*, 2000] was used for the calculations. The model calculates diurnal steady state concentrations of radicals and chemical species by constraining the observed values of ozone, NO, CO, H_2O, NMHCs, and $J(NO_2)$ with the measurements along the flight tracks. It should be noted that the model results are from a local steady state model that does not account for the upwind or downwind photochemical conditions.

[26] Production (P) and loss (L) rates of ozone were calculated using the 10-s merged data for all altitudes but excluding take-off and landing, the polluted air masses from flight 5, and air masses influenced by stratospheric intrusions. The median values for each 1-km altitude step were integrated to derive column rates. A summary of the ozone budget for the 0–13-km column is given in Table 3. Figure 10 also shows median altitude profiles of the calculated diurnal averages of P, L, and the local net ozone production rates (P-L). The tropospheric (0–13 km) column-integrated rate of ozone production is 74×10^{10} molecules cm^{-2} s^{-1}. The average stratospheric fluxes in NH and at midlatitudes in spring have been estimated to be $\sim 3-4 \times 10^{10}$ molecules cm^{-2} s^{-1} and $\sim 10-20 \times 10^{10}$ molecules cm^{-2} s^{-1}, respectively, by global chemical transport models (GCTM) [*Hauglustaine et al.*, 1998; *Wang et al.*, 1998a, 1998b]. The integrated ozone production rate is 3–20 times larger than the stratospheric fluxes, suggesting that photochemical production is a dominant factor for the springtime increase of ozone. The integrated value of P during BIBLE T is comparable to that of 58 molecules cm^{-2} s^{-1} estimated for 20°–30°N during PEM-W-B [*Crawford et al.*, 1997]. Net production of 8×10^{10} molecules cm^{-2} s^{-1} at 0–2 km is larger than that estimated for 20°–30°N during PEM-W-B by a factor of 2. In contrast, the result showed net destruction of ozone at 2–7 km (7×10^{10} molecules cm^{-2} s^{-1}) during BIBLE T, while net production of ozone prevailed at 2–8 km ($\sim 10 \times 10^{10}$ molecules cm^{-2} s^{-1}) during PEM-W-B. However, it should also be noted that the above estimate is not statistically representative of the season because of the limited amount of data below 7 km (Table 3). Especially, the amount of data at 0–2 km is only 7% of the total

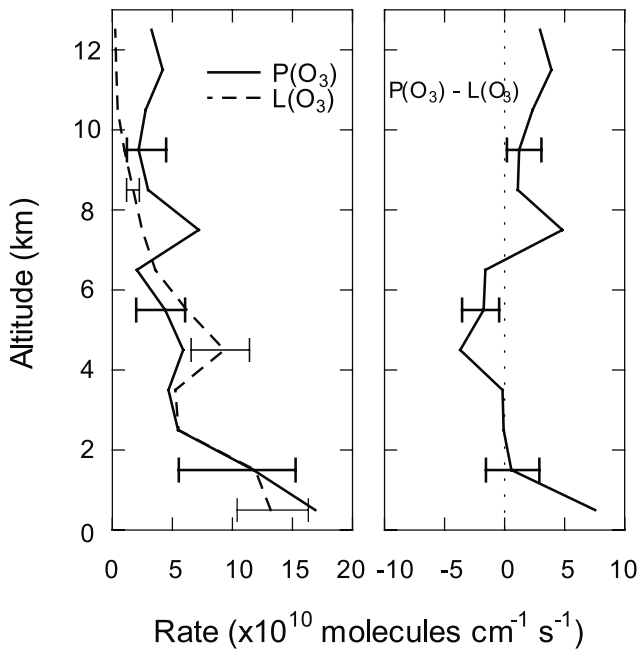

Figure 10. Median altitude profiles of the calculated diurnal-average rates of ozone production (P), destruction (L), and the net ozone production (P-L) for each 1-km altitude step. The values are calculated from 1-min data at solar zenith angles less than 60°. Data points used for the calculation are the same as those in Figure 5. The bars indicate the central 67% values.

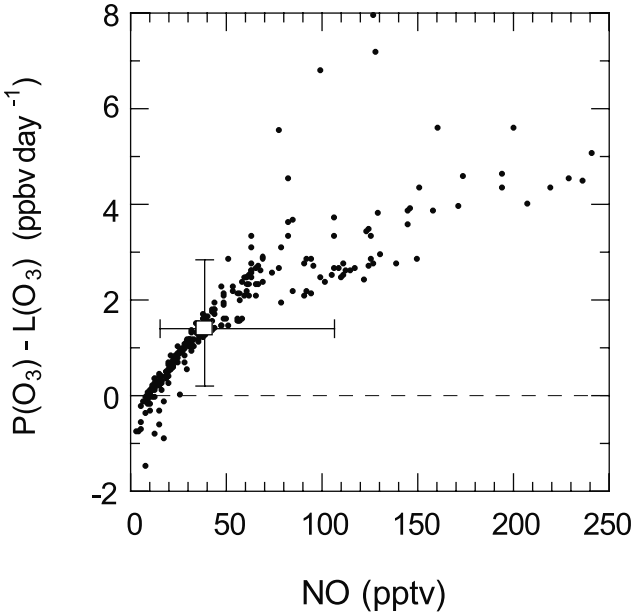

Figure 11. Scatterplot of NO versus diurnal average net ozone production rate at altitudes above 7 km. Data used are the same as those in Figure 5 but for 1-min data at solar zenith angles less than 60° (therefore 6 times fewer points). The median value is also shown with a square.

data. The large variability in P at 0–2 km, combined with the large contribution (40 %) to the column-integrated production rate, leads to reduced statistical reliability in the estimate of the column-integrated production rate.

[27] The median values at 7–13 km show that the P-L values are positive, which correspond to the range of 0.5–4.4 ppbv d^{-1} (0.7–5.1% d^{-1}). Figure 11 shows a scatterplot of the P–L values versus NO at 7–13 km. Critical NO values are defined as the levels of NO at which ozone formation and destruction are balanced [*Crutzen*, 1979]. The critical NO values ranged between 9–13 pptv at 7–13 km during BIBLE T. The median measured NO value at this altitude region was about 40 pptv, which was higher than the critical NO values by a factor of 3–4, indicating the importance of photochemical ozone production on the ozone budget in the upper troposphere in spring. The net production rate in the upper troposphere was also shown to be positive during PEM-W-A and B [*Davis et al.*, 1996; *Crawford et al.*, 1997]. The median net ozone production rate of 1.4 ppbv d^{-1} for 26°–44°N at 7–13 km during BIBLE T is comparable to that of 1.7 ppbv d^{-1} estimated for 20°–30°N at 8–12 km during PEM-W-B [*Crawford et al.*, 1997]. Net ozone production has been shown to prevail in most of the northern midlatitude upper troposphere throughout the year using a GCTM [*Klonecki and Levy*, 1997; *Yienger et al.*, 1999]. The year-round net ozone production in the upper troposphere is compensated for by mixing with lower tropospheric air, where ozone is destroyed in summer and fall. An increase in the total column ozone occurs in winter and spring when net ozone production also occurs in the lower troposphere [*Yienger et al.*, 1999]. Considering the longer photochemical lifetime of ozone in the upper troposphere (2–6 months) [*Wang et al.*, 1998b] than that in the lower troposphere, continuous ozone production in the upper troposphere from winter to spring contributed to the higher ozone values during BIBLE T than those during PEM-W-B. However, net ozone production in the middle and lower troposphere in spring followed by vertical mixing also contributes to the springtime ozone amounts in the upper troposphere. More extensive observations both in the lower and upper troposphere in spring are needed to separate these two effects.

[28] The P-L values in the highly polluted air masses discussed in 3.2 were also estimated to be 3.2–8.5 ppbv d^{-1} (3.4–9.5% d^{-1}), which correspond to the high NO mixing ratios of 160–680 pptv (Table 2). The net diurnal-averaged production rate in these air masses was significantly larger than those in other air masses during BIBLE T and those at 20°–30°N during PEM-W-B, by a factor of 2–4. This result suggests that convective activity over east Asia has a large impact on the ozone levels over the whole Pacific region through eastward transport of ozone precursors.

4. Summary and Conclusions

[29] Aircraft measurements of ozone, NO, NO_y, CO, and NMHCs were made mainly in the upper troposphere at 26°–44°N near Japan during April 1998. The observed ozone mixing ratios were about 80 ppbv at 7–13 km and 60 ppbv at 2–7 km. At all altitude levels, the ozone concentrations during BIBLE T were higher by 10–30 ppbv than those observed during PEM-West B at 20°–30°N. The average ozone values during BIBLE T were very similar to the climatological values obtained by ozonesonde measurements over Japan in April during 1993–1997.

[30] The CO and C_3H_8 mixing ratios below 3 km during BIBLE T were lower than those during PEM-West B, as expected by their seasonal variations. The vertical gradients of these species above 5 km were small during BIBLE T because of active convection in April. In fact, highly polluted air masses were observed in the upper troposphere at 8–11 km over the Japan Sea on 24 April. They were transported from the boundary layer to the upper troposphere by cumulus convection associated with a cold front over northeast China during the 1–2 days prior to sampling.

[31] In air masses not influenced by recent convection over east Asia, NO_x and NO_y were positively correlated with C_3H_8, suggesting significant contributions of anthropogenic activities on the levels of reactive nitrogen. However, other sources of reactive nitrogen, including the effect of NO production by lightning, need to be assessed to quantify the contribution of the surface sources. Ozone was correlated well with NO_y and C_3H_8. The slope of the O_3-NO_y correlation was 3 times smaller than typically found in the lowermost stratosphere. The diurnal-average column-integrated gross production rate of tropospheric ozone, estimated by a photochemical box model, was larger than the NH average and local stratospheric flux at NH midlatitudes in spring by a factor of 3–20. These results demonstrate the dominance of tropospheric photochemistry as a source of ozone over stratospheric input. Although the number of data is limited, the results imply that photochemical production is a dominant factor of the springtime increase of ozone.

[32] The net ozone production rate in these air masses was estimated to be 1–4 ppbv d^{-1} at 7–13 km. The ozone production rate is comparable to that calculated for 20°–30°N in the upper troposphere during PEM-West B. Continuous ozone production in the upper troposphere from winter to spring contributes to the enhancement of the ozone values in April, as observed during BIBLE T relative to those of PEM-West B. In addition, ozone produced in the lower troposphere, where net ozone production prevailed during PEM-West B, can also be transported to the upper troposphere by convection in April. Conversely, ozone produced in the upper troposphere can be transported downward by mixing associated with convection. The relative importance of in situ ozone production in the upper troposphere as compared with transport of ozone from below still needs to be assessed by further measurements.

[33] **Acknowledgments.** The BIBLE project was financially supported by the Earth Observation Research Center (EORC) of the National Space Development Agency of Japan (NASDA). The authors acknowledge the support and efforts of the staff of the Diamond Air Service Co. We are deeply indebted to N. Nishi, M. Fujiwara, and anonymous reviewers for helpful comments and suggestions.

References

Bey, I., D. J. Jacob, J. A. Logan, and R. M. Yantosca, Asian chemical outflow to the Pacific: Origins, pathways and budgets, *J. Geophys. Res.*, *106*, 23,097–23,114, 2001.

Blake, D. R., T.-Y. Chen, T. W. Smith Jr., C. J-.L. Wang, O. W. Wingenter, N. J. Blake, F. S. Rowland, and E. W. Mayer, Three-dimensional distribution of NMHCs and halocarbons over the northwestern Pacific during the 1991 Pacific Exploratory Mission (PEM-West A), *J. Geophys. Res.*, *101*, 1763–1778, 1996.

Blake, N. J., D. R. Blake, T.-Y. Chen, J. E. Collins Jr., G. W. Sachse, B. E. Anderson, and F. S. Rowland, Distribution and seasonality of selected hydrocarbons and halocarbons over the western Pacific basin during PEM-West A and PEM-West B, *J. Geophys. Res.*, *102*, 28,315–28,331, 1997.

Buhr, M., D. Sueper, M. Trainer, P. Goldan, B. Kuster, and F. Fehsenfeld, Trace gas and aerosol measurements using aircraft data from the North Atlantic Regional Experiment (NARE 1993), *J. Geophys. Res.*, *101*, 29,013–29,027, 1996.

Crawford, J., et al., An assessment of ozone photochemistry in the extratropical western North Pacific: Impact of continental outflow during the late winter/early spring, *J. Geophys. Res.*, *102*, 28,469–28,487, 1997.

Crutzen, P. J., The role of NO and NO_2 in the chemistry of the troposphere and stratosphere, *Annu. Rev. Earth Planet. Sci.*, *7*, 443–472, 1979.

Daum, P. H., L. I. Kleinman, L. Newman, W. T. Luke, J. Weinstein-Lloyd, C. M. Berkowitz, and K. M. Busness, Chemical and physical properties of plumes of anthropogenic pollutants transported over the North Atlantic during the North Atlantic Regional Experiment, *J. Geophys. Res.*, *101*, 29,029–29,042, 1996.

Davis, D. D., et al., Assessment of the ozone photochemistry tendency in the western North Pacific as inferred from PEM-West A observations during the fall of 1991, *J. Geophys. Res.*, *101*, 2111–2134, 1996.

Drummond, J. W., D. H. Ehhalt, and A. Volz, Measurements of nitric oxide between 0–12 km altitude and 67°N to 60°S latitude obtained during STRATOZ III, *J. Geophys. Res.*, *93*, 15831–15849, 1988.

Galanter, M., H. Levy II, and G. R. Carmichael, Impacts of biomass burning on tropospheric CO, NO_x, and O_3, *J. Geophys. Res.*, *105*, 6633–6653, 2000.

Gregory, G. L., J. T. Merrill, M. C. Shipham, D. R. Blake, G. W. Sachse, and H. B. Singh, Chemical characteristics of tropospheric air over the Pacific Ocean as measured during PEM-West B: Relationship to Asian outflow and trajectory history, *J. Geophys. Res.*, *102*, 28,275–28,285, 1997.

Hauglustaine, D. A., G. P. Brasseur, S. Walters, P. J. Rasch, J.-F. Müller, L. K. Emmons, and M. A. Carroll, MOZART, a global chemical transport model for ozone and related chemical tracers, 2, Model results and evaluation, *J. Geophys. Res.*, *103*, 28,291–28,335, 1998.

Hoell, J. M., D. D. Davis, S. C. Liu, R. Newell, M. Shipham, H. Akimoto, R. J. McNeal, R. J. Bendura, and J. W. Drewry, Pacific Exploratory Mission-West A (PEM-West A): September–October 1991, *J. Geophys. Res.*, *101*, 1641–1653, 1996.

Hoell, J. M., D. D. Davis, S. C. Liu, R. Newell, H. Akimoto, R. J. McNeal, and R. J. Bendura, The Pacific Exploratory Mission-West Phase B: February–March 1994, *J. Geophys. Res.*, *102*, 28,223–28,240, 1997.

Inoue, T., On the temperature and effective emissivity determination of semi-transparent cirrus clouds by bi-spectal measurements in the 10 μm window region, *J. Meteorol. Soc. Jpn.*, *63*, 88–99, 1985.

Inoue, T., Features of clouds over the tropical Pacific during northern hemispheric winter derived from split window measurements, *J. Meteorol. Soc. Jpn*, *67*, 621–637, 1989.

Jaffe, D., et al., Transport of Asian air pollution to North America, *Geophys. Res. Lett.*, *26*, 711–714, 1999.

Junkerman, W., U. Platt, and A. Volz-Thomas, A photoelectric detector for the measurement of photolysis frequencies of ozone and other atmospheric molecules, *J. Atmos. Chem.*, *8*, 203–227, 1989.

Kita, K., et al., Photochemical production of ozone in the upper troposphere in association with cumulus convection over Indonesia, *J. Geophys. Res.*, *107*, doi:10.1029/2001JD000844, in press, 2002.

Kley, D., J. W. Drummomd, M. McFarland, and S. C. Liu, Tropospheric profiles of NO_x, *J. Geophys. Res.*, *86*, 3153–3161, 1981.

Klonecki, A. A., and H. Levy II, Tropospheric chemical ozone tendencies in $CO\text{-}CH_4\text{-}NO_y\text{-}H_2O$ system: Their sensitivity to variations in environmental parameters and their application to a global chemistry transport model study, *J. Geophys. Res.*, *102*, 21,221–21,237, 1997.

Ko, M., J. Rodriguez, W. Hu, Y. Kondo, M. Koike, K. Kita, S. Kawakami, and D. Blake. Photochemical ozone budget during BIBLE-A campaign, paper presented at The Quadrennial Ozone Symposium, Int. Ozone Comm. and Int. Assoc. for Meteorol. and Atmos. Sci., Sapporo, Japan, 3–8 July 2000.

Koike, M., Y. Kondo, S. Kawakami, H. Nakajima, G. L. Gregory, G. W. Sachse, H. B. Singh, E. V. Browell, J. T. Merril, and R. E. Newell, Reactive nitrogen and its correlation with O_3 and CO over the Pacific in winter and early spring, *J. Geophys. Res.*, *102*, 28,385–28,404, 1997.

Koike, M., et al., Impact of aircraft emissions on reactive nitrogen over the North Atlantic flight corridor region, *J. Geophys. Res.*, *105*, 3665–3677, 2000.

Kondo, Y., H. Ziereis, M. Koike, S. Kawakami, G. L. Gregory, G. W. Sachse, H. B. Singh, D. D. Davis, and J. T. Merrill, Reactive nitrogen over the Pacific Ocean during PEM-West A, *J. Geophys. Res.*, *101*, 1809–1828, 1996.

Kondo, Y., M. Koike, S. Kawakami, H. B. Singh, H. Nakajima, G. L. Gregory, D. R. Blake, G. W. Sachse, J. T. Merrill, and R. E. Newell, Profiles and partitioning of reactive nitrogen over the Pacific Ocean in winter and early spring, *J. Geophys. Res.*, *102*, 28,405–28,424, 1997a.

Kondo, Y., S. Kawakami, M. Koike, D. W. Fahey, H. Nakajima, N. Toriyama, M. Kanada, Y. Zhao, G. W. Sachse, and G. L. Gregory, The performance of an aircraft instrument for the measurement of NO_y, *J. Geophys. Res.*, *102*, 28,663–28,671, 1997b.

Kotamarthi, V. R., et al., Evidence of heterogeneous chemistry on sulfate aerosols in stratospherically influenced air masses sampled during PEM-West B, *J. Geophys. Res.*, *102*, 28,425–28,436, 1997.

Liu, S. C., D. Fley, M. McFarland, J. D. Mahiman, and H. Levy II, On the origin of tropospheric ozone, *J. Geophys. Res.*, *85*, 7546–7552, 1980.

Liu, S. C., et al., Sources of reactive nitrogen in the upper troposphere during SONEX, *Geophys. Res. Lett.*, *26*, 2441–2444, 1999.

Logan, J. A., An analysis of ozonesonde data for the troposphere: Recommendations for testing 3-D models and development of a gridded climatology for tropospheric ozone, *J. Geophys. Res.*, *104*, 16,115–16,149, 1999.

Matuzono, T., T. Sano, and T. Ogawa, Development of the trajectory analysis model (EORC/TAM), *EORC Bull. Tech. Rep. 1*, edited by T. Igarashi, pp. 55–68, Natl. Space Dev. Agency of Jpn., Tokyo, 1998.

Merrill, J. T., Atmospheric long range transport to the Pacific Ocean, in *Chemical Oceanography*, edited by J. P. Riley and R. Duce, pp. 15–50, Academic, San Diego, Calif., 1989.

Murphy, D. M., D. W. Fahey, M. H. Proffitt, S. C. Liu, K. R. Chan, C. S. Eubank, S. R. Kawa, and K. K. Kelly, Reactive nitrogen and its correlation with ozone in the lower stratosphere and upper troposphere, *J. Geophys. Res.*, *98*, 8751–8773, 1993.

Newell, R. E., E. V. Browell, D. D. Davis, and S. C. Liu, Western Pacific tropospheric ozone and potential vorticity: Implications for Asian pollution, *Geophys. Res. Lett.*, *24*, 2733–2736, 1997.

Novelli, P. C., K. A. Masarie, P. P. Tans, and P. M. Lang, Recent changes in atmospheric carbon monoxide, *Science*, *263*, 1587–1590, 1994.

Novelli, P. C., K. A. Masarie, and P. M. Lang, Distributions and recent changes of carbon monoxide in the lower troposphere, *J. Geophys. Res.*, *103*, 19,015–19,033, 1998.

Ridley, B. A., J. G. Walega, J. E. Dye, and F. E. Grahek, Distributions of NO, NO_x, NO_y, and O_3 to 12 km altitude during the summer monsoon season over New Mexico, *J. Geophys. Res.*, *99*, 25,519–25,534, 1994.

Ridley, B. A., E. L. Atlas, J. G. Walega, G. L. Kok, T. A. Staffelbach, J. P. Greenberg, F. E. Grahek, P. G. Hess, and D. D. Montzka, Aircraft measurements made during the spring maximum of ozone over Hawaii: Peroxides, CO, O_3, NO_y, condensation nuclei, selected hydrocarbons, halocarbons, and alkylnitrates between 0.5 and 9 km altitude, *J. Geophys. Res.*, *102*, 18,935–18,961, 1997.

Sandholm, S., S. Smith, R. Bai, and J. Bradshaw, Recent and future improvements in two-photon laser-induced fluorescence NO measurement capabilities, *J. Geophys. Res.*, *102*, 28,651–28,661, 1997.

Smyth, S. B., et al., Comparison of free tropospheric western Pacific air mass classification schemes for the PEM-West A experiment, *J. Geophys. Res.*, *101*, 1743–1762, 1996.

Talbot, R. W., et al., Chemical characteristics of continental outflow from Asia to the troposphere over the western Pacific Ocean during February–March 1994: Results from PEM-West B, *J. Geophys. Res.*, *102*, 28,255–28,274, 1997.

Talbot, R. W., et al., Reactive nitrogen budget during the NASA SONEX mission, *J. Geophys. Res.*, 3057–3060, 1999.

van Aardenne, J. A., G. R. Carmichael, H. Levy II, D. Streets, and L. Hordijk, Anthropogenic NO_x emissions in Asia in the period 1990–2020, *Atmos. Environ.*, *33*, 633–646, 1999.

Wang, Y., J. A. Logan, and D. J. Jacob, Global simulation of tropospheric O_3-NO_x-hydrocarbon chemistry, 2, Model evaluation and global ozone budget, *J. Geophys. Res.*, *103*, 10,727–10,755, 1998a.

Wang, Y., D. J. Jacob, and J. A. Logan, Global simulation of tropospheric O_3-NO_x-hydrocarbon chemistry, 3, Origin of tropospheric ozone and effects of nonmethane hydrocarbons, *J. Geophys. Res.*, *103*, 10,757–10,767, 1998b.

Weinheimer, A. J., J. G. Walega, B. A. Ridley, G. W. Sachse, B. E. Anderson, and J. E. Collins Jr., Stratospheric NO_y measurements on the NASA DC-8 during AASE II, *Geophys. Res. Lett.*, *20*, 2563–2566, 1993.

Yienger, J. J., A. A. Klonecki, H. Levy II, W. J. Moxim, and G. R. Carmichael, An evaluation of chemistry's role in the winter-spring ozone maximum found in the northern midlatitude troposphere, *J. Geophys. Res.*, *104*, 3655–3667, 1999.

D. R. Blake, Department of Chemistry, University of California, Irvine, CA 92697, USA.

W. Hu and M. Ko, Atmospheric and Environmental Research, Inc., 131 Hartwell Avenue, Lexington, MA 02421-3126, USA.

S. Kawakami and T. Ogawa, Earth Observation Research Center, National Space and Development Agency of Japan, Tokyo 106, Japan. (kawakami@eorc.nasda.go.jp)

K. Kita, Y. Kondo, and Y. Miyazaki, Research Center for Advanced Science and Technology, University of Tokyo, 4-6-1 Komaba, Meguro-ku, Tokyo 153-8904, Japan. (kita@atmos.rcast.u-tokyo.ac.jp; kondo@atmos.rcast.u-tokyo.ac.jp; yuzom@atmos.rcast.u-tokyo.ac.jp)

M. Koike, Earth and Planetary Science, Graduate School of Science, University of Tokyo, Tokyo 113-0033, Japan. (koike@eps.s.u-tokyo.ac.jp)